Bone regeneration in Ds-Red pig calvarial defect using allogenic transplantation of EGFP-pMSCs – a comparison of host cells and seeding cells in the scaffold

Short title: *In vivo* comparison of host cells and seeding cells

Ming-Kai Hsieh[1,2,3,4], Chia-Jung Wu[2,3] , Xuan-Chun Su [5], Yi-Chen Chen[1,5,6], Tsung-Ting Tsai[2,3,4], Chi-Chien Niu[2,3,4], Po-Liang Lai[2,3,4] * ,Shinn-Chih Wu [1,5,6]*

[1]Institute of Biotechnology, National Taiwan University, Taipei, Taiwan.

[2]Department of Orthopaedic Surgery, Chang Gung Memorial Hospital, Taoyuan, Taiwan

[3]Bone and Joint Research Center, Chang Gung Memorial Hospital, Taoyuan, Taiwan

[4]College of Medicine, Chang Gung University, Taoyuan, Taiwan

[5]Department of Animal Science and Technology, National Taiwan University, Taipei, Taiwan.

[6]Center for Biotechnology, National Taiwan University, Taipei, Taiwan.

* Shinn-Chih Wu and Po-Liang Lai are co-corresponding authors

Corresponding authors:

Dr. Po-Liang Lai

Department of Orthopaedic Surgery, Chang Gung Memorial Hospital, No. 5, Fu-Shing St., Kweishan, Taoyuan 33305, Taiwan

Tel: +886-3-328-1200 ext. 3612 Fax: +886-3-327-8113

Email: polianglai@gmail.com

Dr.Shinn-Chih Wu

Institute of Biotechnology, National Taiwan University, Taipei, Taiwan, R.O.C.

Center for Biotechnology, National Taiwan University, Taipei, Taiwan, R.O.C.

Department of Animal Science and Technology, National Taiwan University, Taipei, Taiwan, No.50, Lane 155, Sec. 3, Kee-lung Road, Taipei,10672, Taiwan,. Tel: +886-2-33664147, Fax: +886-2-27324070, E-mail: scw01@ntu.edu.tw

Keywords: mesenchymal stem cell, bone regeneration, enhanced green fluorescent, DsRed pig, pig calvarial defect model

Abstract

Background: Cells, scaffolds, and factors are the triad of regenerative engineering; however, it is difficult to distinguish whether cells in the regenerative construct are from the seeded cells or host cells via the host blood supply. We performed a novel *in vivo* study to transplant enhanced green fluorescent pig mesenchymal stem cells (EGFP-pMSCs) into calvarial defect of DsRed pigs. The cell distribution and proportion were distinguished by the different fluorescent colors through the whole regenerative period.

Method/Results: Eight adult domestic Ds-Red pigs were treated with five modalities: empty defects without scaffold (group 1); defects filled only with scaffold (group 2); defects filled with osteoinduction medium-loaded scaffold (group 3); defects filled with 5 x 10^3 cells/scaffold (group 4); and defects filled with 5 x 10^4 cells/scaffold (group 5). The *in vitro* cell distribution, morphology, osteogenic differentiation, and fluorescence images of groups 4 and 5 were analyzed. Two animals were sacrificed at 1, 2, 3, and 4 weeks after transplantation. The *in vivo* fluorescence imaging and quantification data showed that EGFP-pMSCs were represented in the scaffolds in groups 4 and 5 throughout the whole regenerative period. A higher seeded cell density resulted in more sustained seeded cells in bone regeneration compared to a lower seeded cell density. Host cells were recruited by seeded cells if enough space was available in the scaffold. Host cells in groups 1 to 3 did not change from the 1st week to 4th week, which

indicates that the scaffold without seeded cells cannot recruit host cells even when enough space is available for cell ingrowth. The histological and immunohistochemical data showed that more cells were involved in osteogenesis in scaffolds with seeded cells.

Conclusion: Our *in vivo* results showed that more seeded cells recruit more host cells and that both cell types participate in osteogenesis. These results suggest that scaffolds without seeded cells may not be effective in bone transplantation.

Introduction

Skeletal defects require surgery using bone grafts. Autografts are the gold standard for bone grafting [1]; however, donor site morbidity and the limited amount of available donor tissue restrict their application [2, 3]. Regenerative tissue engineering using cells, scaffolds, factors and blood supply [4] has become an alternative method to treat skeletal bone defects.

Allografts may provide the same osteoconductive conduit for bony fusion as traditional autografts and may have comparable biomechanical properties without amount restriction [5, 6]. Although depleted of osteoprogenitor cells like mesenchymal stem cells (MSCs), the fusion rate still reaches 73% to 100% in instrumented spinal fusion [7-16], making allograft a clinically feasible alternative form of fusion. The role of cells in allograft prompted us to wonder if seeded cells are necessary in bone regeneration clinically.

MSCs are undifferentiated multipotent cells with the capacity to differentiate into osteoblasts, chondrocytes, adipocytes, fibroblasts, and other tissues of mesenchymal origin [17]. MSCs lack expression of costimulatory molecules like CD40, CD80, and CD86, which makes them largely non-immunogenic [18], as supported by evaluations of their immunosuppressive properties using mitogen proliferation assays [19]. Due to these suitable transplantation properties, MSCs are an important material in developmental biology and transgenic methods, as well as in potential clinical applications in tissue engineering and gene therapy [20, 21].

Some studies have found that seeded MSCs may be capable of releasing major growth factors, reducing the immune response, mobilizing the host's cells or eventually directly

differentiating into osteoblasts [22-25]. The expansion, proliferation, migration, viability and osteogenic differentiation of MSCs on different types of scaffolds have been shown in studies [26-31], but the role of seeded MSCs is still poorly addressed. Histologically, it is difficult for us to distinguish cells in the regenerative construct from seeded MSCs or from host MSCs via the host blood supply. In this study, we transplanted EGFP pig MSCs into calvarial defect of DsRed pigs. The cell distribution and proportion were distinguished by different fluorescent colors throughout the whole regenerative period.

The purpose of the present study was to clarify the distribution and proportion of seeded cells and host cells by tracking two fluorescent cells in the same scaffold in a pig critical-sized calvarial defect model.

Materials and methods

EGFP-pMSCs culture in the scaffold

Scaffold

A hemostatic gelatin sponge, Spongostan™ (Ferrosan Medical Device, MS0003, thickness 0.1 cm), was used as the 3D scaffold [32]. Scanning electron microscopy (SEM) (Hitachi, SU8220) analysis indicated a mean pore size of approximately 148 ± 62 μm (Fig 1). To perform transplantation, the scaffolds were cut into disks with a diameter of 0.8 cm, sterilized by

75 % (v/v) ethanol and washed three times with phosphate-buffered saline. The sterile scaffold disks were then immersed in Opti-MEM medium (Gibco) before use.

Fig 1. Morphology of the scaffold. The Hemostatic Gelatin Sponge, SpongostanTM (Ferrosan Medical Device, MS0003, Thickness 0.1 cm) was used as the 3D Scaffold and determined by SEM (Scanning Electron Microscopy) to have a mean pore size of approximately 148 ± 62 μm. Increased magnification was observed from A to C.

Cell culture

Passage 5 EGFP-pMSCs [19] were cultured in minimum essential medium alpha (MEM-α) (Gibco) supplemented with 10% fetal bovine serum (HyClone) and antibiotic solutions (100 U/mL penicillin, 100 μg/mL streptomycin, 50 μg/mL gentamicin and 250 ng/mL fungizone) (Gibco). The cells were maintained in a humidified 37 ℃ incubator supplied with 5 % CO_2.

Seeding of cells

The sterile scaffold disks were individually placed onto the wells of a 48 well-plate. The cell seeding density was 5 x 10^3 or 5 x 10^4 cells/disk. Cells in 50 μL of medium were seeded throughout the surface of the scaffold disk and incubated for 3 hours to allow cell attachment before the addition of medium. The culture condition was observed by fluorescent microscopy and recorded until the 28th day after seeding onto scaffolds.

In vitro cell distribution and morphology analysis

The cell scaffold constructs were washed twice with phosphate buffered saline (PBS; GIBCO™, Invitrogen Corp., Carlsbad, CA) and fixed in 1.5% v/v glutaraldehyde in 0.14M sodium cacodylate (pH 7.4) for 30 mins at room temperature. Dehydration was performed by sequential immersion in serial diluted ethanol solutions of 50, 60, 70, 80, 90, and 100% v/v. The samples were then transferred to hexamethyldisilazane and air-dried at room temperature overnight. The cell distribution and morphology were analyzed by SEM and confocal laser scanning microscopy (CLSM) (Bio-Rad MRC 600).

In vitro osteogenic differentiation

The above two groups then received 0.5 mL/well of osteogenic induction medium (OIM) to promote cell differentiation. The OIM medium was composed of complete MEM-α medium enriched with 10^{-7} M dexamethasone (Sigma), 10 mM β- glycerophosphate (Sigma) and 50 μg/mL ascorbic acid (Sigma) [32]. The OIM medium was replenished every two or three days for a total of 7 days. The osteogenic potential was assessed using an alkaline phosphatase staining and Alizarin red S (ARS) staining.

Alkaline phosphatase staining and quantification

The osteogenic potential was assessed using an ALP assay kit (BioVision K412-500) after 7 days. The cells were washed twice with ice-cold PBS and lysed using 300 µL of RIPA

(radioimmunoprecipitation assay) lysis buffer (Sigma-Aldrich Corp., St Louis, MO, USA) for 5 mins on ice. The cells were then rapidly scraped from the plate, and the cell lysates/RIPA buffer were transferred to a 1.5-mL microcentrifuge tube on ice for 20 min, followed by centrifugation at 8000 g for 10 min at 4 °C. The supernatant was then added to a new 1.5-mL microcentrifuge tube and stored at -20 °C. 50 μL of 5 mM pNPP solution was added to each well containing the test samples and the aliquots were incubated for 60 min at 25 °C while protected from light. Subsequently, 20 μL of the stop solution was added to terminate the ALP activity in the sample. The absorbance at 405 nm was measured with a spectrophotometer (UV-Vis 8500). Then, the ALP activity was calculated using the following formula: ((optical density –mean optical density of the control wells) × total volume × dilution)/(18.45 × sample volume).

Alizarin red S (ARS) staining and quantification

Cells cultured on the discs at different time points were washed twice with PBS and fixed with 4% paraformaldehyde for 15 min. The fixative was removed, and the discs with cells were rinsed with deionized water. The scaffolds were stained with a 2% ARS staining kit (ScienCell) for 5 mins to clarify the calcium deposits. The staining solution was discarded, and the scaffolds were carefully washed with deionized water to remove excess stain. The staining results were captured with a digital camera. To quantify the staining of each scaffold, 1 mL/disc of 10 wt% cetylpyridinium chloride (Sigma) was added to the discs. The discs were left on an orbital shaker (speed, 60 rpm) for 1 h to completely resolve the dye from the discs. Finally, 100 μL of the

156 dissolved solution from each scaffold was placed into a well of a 96-well plate, and the
157 absorbance was measured at 540 nm with an ELISA reader.

158

159 ## *In vivo* experimental design

160 Eight adult domestic Ds-Red pigs (average age of 15 ± 3months) with a mean weight of
161 100 ±20 kgs were obtained from the Department of Animal Science, National Taiwan University
162 (Taipei, Taiwan). This study was carried out in strict accordance with the recommendations in
163 the *Guide for the Care and Use of Laboratory Animals* of the National Institutes of Health. All
164 animals were used under approved animal protocols by the Institutional Animal Care and Use
165 Committee of National Taiwan University (NTU107-EL-00128) and housed accordingly.

166 The five treatment modalities were empty defects without scaffold (group 1; n=1);
167 defects filled with only scaffold (group 2; n=1); defects filled with osteoinduction medium-
168 loaded scaffold (group 3; n=1); defects filled with 5 x 10^3 cells/scaffold (group 4; n=2) and
169 defects filled with 5 x 10^4 cells/scaffold (group 5; n=2).

170 Seven defects were created in each animal. The treatment modalities of the defects were
171 determined for each animal separately by a randomization chart.

172

173 ## Operation

174 Zoletil® (5 mg/kg body weight) was injected in the neck area of the pig intramuscularly
175 as a sedative. All experimental procedures were performed under a standard anesthetic/ analgesic

176 protocol as described in previous studies [19, 33].

177 The frontal bone was exposed after a standard sagittal approach in the forehead region.
178 Identical bony defects were then created with a saline-cooled trephine burr (diameter 8 mm,
179 depth 2 mm) meeting the requirements for a critical size defect in pigs [34]. The defects were
180 positioned at least 5 mm apart to minimize biological interactions [35]. The internal plate of the
181 neurocranium remained completely intact during the procedure. After well hemostasis, the
182 scaffold was implanted (Fig 2). The periosteum and skin over the defects were sutured in two
183 layers with resorbable material (Vicryl USP 3-0; Vicryl USP1-0; Ethicon Johnson & Johnson,
184 NJ, USA).

185 **Fig 2. Critical-sized calvarial defects of DsRed pig were created.** The frontal bone was
186 exposed after a standard sagittal approach in the forehead region. Seven identical bony defects
187 were created in the frontal bone and the defects were positioned at least 5mm apart to minimize
188 biological interactions. The internal plate of the neurocranium remained completely intact during
189 the procedure. After adequate hemostasis, the scaffolds were implanted.

190

191 Sacrifice and preparation of specimens

192 Two animals were sacrificed 1, 2, 3, and 4 weeks after transplantation. The animals were
193 anesthetized by intramuscular injection of tiletamine-zolazepam and atropine and then were
194 euthanized with a lethal injection of sodium pentobarbital. The frontal bone was en bloc resected,
195 and the calvarial defects were retrieved separately using an oscillating autopsy saw. The

196 retrieved specimens were fixed in 10% neutral formalin for further survey.

197

198 ## *In vivo* fluorescence imaging

199 All samples were washed twice with PBS, fixed in 4% v/v formaldehyde (methanol-free;
200 Polyscience) for 15 min, permeabilized with 0.1% v/v Triton X-100 for 5 min, and incubated in
201 10 mg/mL bovine serum albumin and 100 g/mL RNase for 45 min at room temperature. F-actin
202 filaments were stained with Alexa Fluor-conjugated phalloidin (Molecular Probes) for 20 min,
203 and nuclei were counterstained with 10 g/mL propidium iodide (Sigma) for 10 min. Finally, the
204 samples were washed with PBS and mounted in Vectashield®. CLSM images were acquired on
205 a BioRad MRC 600 microscope. The quantitative distribution of the two types of fluorescent
206 cells was analyzed by using NIH Image J software (National Institutes of Health, USA) and
207 presented as the modified integrated density (Modified IntDen). The modified integrated density
208 was calculated based on the selected Integrated Density - (Area of selected cell ×Mean
209 fluorescence of background readings).

210

211 ## Histology

212 The tissue samples were processed to obtain non-decalcified ground sections. After 2
213 weeks in 10% neutral formalin, the specimens were rinsed in running tap water, trimmed,
214 dehydrated in ascending concentrations of ethanol, and embedded in methyl methacrylate. The
215 embedded tissue blocks were serially cut into 5-µm-thick ground sections using a microtome

(Leica SM 2000; Germany) and mounted on glass slides. Ten cross-sections from the middle of each implant were stained with hematoxylin-eosin and Masson's trichrome and visualized using an optical microscope (DXM200F Digital Camera; Nikon, Tokyo, Japan).

Immunohistochemistry of CD68

After fixation in formalin, the dissected blocks were decalcified for 11 days in 10% EDTA and subsequently embedded in paraffin. In brief, after removal of the embedding material, endogenous peroxidases were blocked with H_2O_2. Semi-thin sections were rinsed in saline and incubated in phosphate-buffered citrate solution, pH 7.4 (Sigma-Aldrich Corp., St Louis, MO, USA), for 20 min in the microwave and rinsed with phosphate-buffered saline. A microtome was used to obtain 3-mm-thick sections. Immunohistochemistry analysis of tissue labelled with anti-CD68 was performed with purified ab81289 (Abcam Inc., Cambridge, MA) at 1:250. Heat-mediated antigen retrieval was performed using Tris/EDTA buffer pH 9.0 (Abcam Inc., Cambridge, MA). Goat Anti-Rabbit IgG H&L (HRP) was used as the secondary antibody at 1/500. The negative control used PBS instead of the primary antibody, and counterstaining was performed with hematoxylin. The qualitative analysis was performed using a light microscope (Nikon Eclipse E600).

Statistical analysis

All experimental results are expressed as the mean ± SD, and the statistical analysis was

236 performed using Student's t-test and two-way ANOVA. Analysis of variance (ANOVA) was
237 performed by using Statistica 6.0 software (Statsoft, Tulsa, OK, USA). Differences with a p
238 value of < 0.05 were considered statistically significant.
239
240 # Results
241
242 ## *In vitro* characterization of EGFP-pMSCs
243 Passage 5 EGFP-pMSCs [20] were collected by incubation with 0.25% trypsin-EDTA for
244 5 min at 37°C and re-suspended in ice-cold washing buffer consisting of PBS with 2% FBS.
245 Phase-contrast images of EGFP-MSCs showed a change from a round-shaped to a spindle-
246 shaped morphology after culture for 1 day. After 2 days of culture, 90% confluence was reached,
247 and the cells were trypsinized and re-plated at a dilution of 1:3. These EGFP-pMSCs proliferated
248 rapidly and harbored a greater abundance of EGFP expression by fluorescence microscopy (Fig
249 3).
250 **Fig 3. Cell culture of EGFP-MSCs.** Phase-contrast image of passage 5 EGFP-MSCs showing
251 the change from round-shaped to spindle-shaped morphology after culture for 1 day (Upper
252 Row). After 2 days of culture, 90% confluence was reached, and the cells were trypsinized and
253 re-plated at a dilution of 1:3. These EGFP-pMSCs proliferated rapidly and harbored a greater
254 abundance of EGFP expression according to fluorescence microscopy (lower row).
255

In vitro fluorescence evaluation

The sterile scaffolds were individually placed onto the wells of a 48 well-plate. The cell seeding density was 5 x 10^3 or 5 x 10^4 cells/scaffold in 50 μL of medium, and the cells were seeded throughout the top side of the scaffold and then incubated for 3 h to allow cell attachment before adding the maintenance medium. From day 3, osteoinduction medium was added, and increasing expression of green fluorescence from day 3 to day 28 was observed in both groups by fluorescent microscopy, especially in the 5 x 10^4 group (Fig 4).

Fig 4. *In vitro* fluorescence evaluation of two different loading density in the scaffolds. An increase in the expression of green fluorescence was observed from day 3 to day 28 in both groups by fluorescence microscopy, especially in the 5 x 10^4 group.

In vitro cell distribution and morphology analysis

SEM analysis showed that this biodegradable and biocompatible scaffold [36] with a mean pore size of approximately 148 ± 62 μm was suitable for growth of the EGFP-pMSCs. The intensity of live cells increased from day 3 to 28, indicating sufficient intricate space available for ingrowth. SEM images indicated that the EGFP-pMSCs spread on the sponge, and cellular extension and networks were observed. The connected pores were nearly covered by cells by day 21 in the 5×10^4 group and by day 28 in the 5×10^3 group (Fig 5). CLSM images of the *in vitro* distribution of EGFP-pMSCs in the scaffolds were obtained from day 3 to day 28 (Fig 6). The constructs were washed with PBS and mounted in Vectashield®. CLSM images were acquired

on a BioRad MRC 600 microscope (100X). Three-dimensional z-stack images were evaluated and merged. The distribution of green fluorescence in both groups corresponded to the cell density, especially in the surface view (Fig 6A). In the cross section of the scaffold (Fig 6B), cells were distributed into the scaffold from the surface to the center from day 3 to day 28. On day 28, more cells were observed in the central area in the 5×10^4 group than the 5×10^3 group, and the space seemed to be sufficient for cell growth in both groups.

Fig 5. *In vitro* SEM analysis. SEM images indicated that the EGFP-pMSCs (yellow heads) spread on the sponge, and cellular extension and networks between them were observed from day 7 to day 28 in both groups. The connected pore was nearly covered by cells at day 21 in the 5×10^4 group and day 28 in the 5×10^3 group.

Fig 6. CLSM images of the *in vitro* distribution of EGFP-pMSCs in the scaffolds. The green fluorescence distribution in both groups corresponded to the cell density, especially in the surface view (A). In the cross section of the scaffold (B), cells were distributed into the scaffold from the surface to the center from day 3 to day 28.

In vitro osteogenic differentiation

Alkaline phosphatase staining and quantification

The alkaline phosphatase staining results on the culture plates were observed by microscopy (Fig 7A). Both groups showed slight positive staining on day 7, and the relative

staining intensity increased on days 14, 21, and 28 compared to days 0 and 7 in the 5×10^3 cell group. In the 5×10^4 cell group, the staining intensity increased significantly from day 7. In both groups, the staining intensity continued to slowly increase steadily from day 21 to day 28. Alkaline phosphatase is an early marker of bone formation, and the level increased significantly in the first 2 weeks, followed by a slow steady increase until day 28. Alkaline phosphatase activity (Fig 7B) showed that the cells seeded in the two groups were able to produce alkaline phosphatase on days 7, 14, 21, and 28, and the enzyme activity was significantly higher in the 5×10^4 group than the 5×10^3 group between days 7 and 28 (** $p < 0.01$, *** $p < 0.001$), indicating higher osteoblast differentiation in the 5×10^4 group.

Fig 7. Alkaline phosphatase staining and quantification analysis

Microscopy observation of alkaline phosphatase staining results on the culture plates (A). Both groups showed slight positive staining on day 7, and the relative staining intensity increased on days 14, 21, and 28 compared to Days 0 and 7 in the 5×10^3 cell group. In the 5×10^4 cell group, the staining intensity increased significantly from day 7. Alkaline phosphatase activity (B) showed the enzyme activity was significantly higher in the 5×10^4 group than the 5×10^3 group from days 7 to 28 (** $p < 0.01$, *** $p < 0.001$), indicating higher osteoblast differentiation in the 5×10^4 group. Data is shown as mean ± standard deviation.

Alizarin red S (ARS) staining and quantification

Alizarin red S staining (Fig 8A) is indicative of bone mineralization and was negative on

316 day 7 in both groups. Up to day 14, all groups showed positive staining with a deep red color,
317 indicating bone nodule formation. The alizarin red staining quantification assay (Fig 8B) was
318 performed at different time points, and the absorbance was measured at 540 nm using an ELISA
319 reader. The absorbance value significantly increased from day 7 to days 14, 21 and 28. The
320 values were significantly higher in the 5×10^4 group than in the 5×10^3 group on day 14 and 21
321 ($p<0.05$), consistent with the results of alkaline phosphatase staining.

322 **Fig 8. Alizarin red S staining and quantification analysis**

323 Alizarin red S staining (A) was negative on day 7 in both Groups. Up to day 14, all groups
324 showed positive staining with deep red color, indicating bone nodule formation. Alizarin red
325 staining quantification assays (B) were performed at different time points. The absorbance value
326 increased significantly from day 7 to days 14, 21 and 28. The values were significantly higher in
327 the 5×10^4 group than in the 5×10^3 group on day 14 and 21. Differences considered significant at
328 * $p< 0.05$ were marked. Data is shown as mean ± standard deviation.

329

330 ## *In vivo* fluorescence imaging

331 Confocal laser scanning microscopy was performed to image groups 1 through 5 from
332 week 1 to week 4. (Fig 9). EGFP-pMSCs were present in the scaffolds in groups 4 and 5 through
333 the whole period. Although the EGFP expression decreased in the third and fourth weeks, DsRed
334 expression increased in groups 4 and 5. The green fluorescence was higher in group 5 than in
335 group 4 at each time point, similar to the *in vitro* fluorescence imaging results (Fig 6A).

DsRed expression was significantly higher in groups 2 and 3 than in group 1 at each time point, which indicated that the empty scaffold facilitates DsRed cells ingrowth. Even at week 4, no sufficient two fluorescent cells were observed in group 1, which indicates that this type of calvarial defect cannot heal spontaneously during the bone healing period used in our experiments.

Fig 9. CLSM image of group 1 to 5 from week 1 to week 4. EGFP-pMSCs were present in the scaffolds in groups 4 and 5 from week 1 to week 4. Although EGFP expression decreased in the third and fourth weeks, DsRed expression was increased in groups 4 and 5. Green fluorescence was higher in group 5 than in group 4 at each time point, similar to the *in vitro* fluorescence distribution result. DsRed expression was significantly higher in groups 2 and 3 than in group 1 at each time point, which indicated that the empty scaffold facilitates DsRed cells ingrowth. Even at week 4, no sufficient two fluorescent cells were observed in group 1.

In vivo fluorescence quantification

The modified integrated density of green and DsRed fluorescence in the acquired images was measured using Image J and expressed as bar graphs (Fig 10). EGFP expression (Fig 10A) was higher in Groups 4 and 5 than in the other three groups from the 1st week to the 3rd week (p<0.05; p<0.01) and was significantly highest in group 5 in the 4th week (p<0.05). These results indicate that the seeded cells were present in the scaffold and that the higher load of seeded cells

356 was sustained until the 4th week. The results of the *in vivo* study were compatible with those of
357 the *in vitro* study. By the 4th week, EGFP expression in Group 4 decreased to the levels in
358 Groups 1-3, which means that an insufficient number of seeded cells may not be effective for
359 tissue transplantation. EGFP expression was highest in the 2nd week, which means that the
360 proliferation of seeded cells reached its highest peak, consistent with the *in vitro* ALP/ARS
361 staining results (Figs 7 and 8).

362 In the 1st week, DsRed expression (Fig 10B) was higher in Group 4 than in the other
363 groups, indicating that recruitment of host cells was facilitated by the scaffold seeded with a
364 lower density of cells compared with the empty scaffold or scaffold seeded with a higher density
365 of cells. DsRed expression decreased from the 1st week to 4th week in group 4 but increased in
366 group 5, which means that more EGFP pMSCs can recruit more host cells 2 weeks after
367 transplantation and that enough available space and higher cell loading can benefit tissue
368 regeneration. The DsRed expression in groups 1 to 3 did not increase from the 1st week to 4th
369 week, indicating that the empty scaffold attracted host cells only in the first week after
370 transplantation and implying that scaffolds without seeded cells may not be effective for tissue
371 transplantation. Osteogenic differentiation may be responsible for the decreased expression of
372 EGFP and DsRed expression from week 2 to week 4 in groups 4 and 5.

373 **Fig 10. *In vivo* fluorescence quantification.**

374 EGFP (A) and DsRed (B) expression using Modified IntDen in Group 1 to 5 from week 1 to 4
375 were demonstrated as bar chart. Differences considered significant at * $p < 0.05$, ** $p < 0.01$, and

376 *** $p < 0.001$ respect to control. Data is shown as mean ± standard deviation.

377

378 Histological analysis

379 Hematoxylin and eosin staining and Masson's trichrome staining were analyzed using a
380 light microscope at various levels of magnification.

381 A greater number of cells were stained with H&E in groups 4 and 5 compared to groups
382 1-3 in the first week (Figs 11). In the fourth week, obvious deposition of osteoids (yellow
383 arrowhead) was noted in group 5. Calcification of the osteoids led to the formation of primitive
384 trabecular bone in group 5 compared with group 4 in the fourth week. In Groups 1-3, cells were
385 sustained until the fourth week, but no obvious osteoids were found in the 4th week.

386 **Fig 11. *In vivo* Hematoxylin and eosin staining.** A greater number of cells were stained
387 with H&E in groups 4 and 5 compared to groups 1-3 in the first week (yellow arrow).Osteoid
388 formation was confirmed histologically in the hematoxylin and eosin-stained defect of group 4
389 and 5 at 4 weeks postoperatively (yellow arrowhead). Staining was observed in all groups in
390 400× magnification.

391 Masson's trichrome staining of cells increased in all groups in week 1 through 4, but
392 blue-colored osteoid-like tissue was only found in groups 4 and 5 after the third week (Fig 12).
393 In the 4th week, connective fibrous tissue with a large amount of undifferentiated cells was noted
394 in groups 1, 2, and 3 (yellow arrowhead). Meanwhile, in groups 4 and 5, thick dense fibrous
395 connective tissue with differentiated osteoblast-like cells (yellow arrow) was noted.

396 **Fig 12. *In vivo* Masson's trichrome staining.** Blue-colored osteoid-like tissue was only
397 found in groups 4 and 5 after the third week. In the 4th week, in groups 4 and 5, thick dense
398 fibrous connective tissue with differentiated osteoblast-like cells (yellow arrow) was noted but
399 only a large amount of undifferentiated cells (yellow arrowhead) without obvious blue-colored
400 osteoid-like tissue in groups 1, 2, and 3 . Staining was observed in all groups in 400×
401 magnification.

402

403

404 ## Immunohistochemistry of CD68

405 The levels of the macrophage marker [37] CD68 were higher in groups 4 and 5 than in
406 the other groups in the fourth week (Fig 12), especially around the neovascularization area. The
407 increase in macrophages indicated an increase in osteoclasts and, consequently, more
408 osteogenesis in groups 4 and 5.

409 **Fig 12. Immunohistochemistry of CD 68.** The macrophage marker were stained with anti-
410 CD68 antibody and marked with yellow arrow in group 4 and 5 in week 4. The increasing
411 arrows, CD 68, in group 5 than group 4 suggested that more neovascularization and thus more
412 osteogenesis in group 5 than group 4 .

413 # Discussion

414 Allografts may provide the same osteoconductive conduits for bony fusion as traditional
415 autografts and may have comparable biomechanical properties [5, 6]. Although depleted of

osteoprogenitor cells like MSCs, the fusion rate still reaches 73% to 100% in instrumented spinal fusion [7-16], making allografts a clinically feasible alternative for fusion. Cells, scaffolds, and factors are the triad of regenerative engineering, and the lack of one of these three graft properties made us wonder about the role of seeded cells in bone regeneration.

A number of studies examining the combination of MSCs and 3-D scaffolds in bone regeneration have reported promising outcomes in animal critical size bone defects [38-43]. These studies aimed to achieve the final result of bone repair by using different kinds of scaffolds [44], sources of MSCs [45] or loaded factors [46-48], but very few studies have focused on the role of the seeded cells.

Kuznetsova et al. [49] used allogenic transplantation of mice MSCs loaded on fabricated 3-D scaffolds made from poly (D, L)-lactic acid and hydroxyapatite in the calvarial defect. They divided the mice into two experimental groups: GFP (+) mice MSCs transplanted into GFP (-) mice and GFP(-) mice MSCs transplanted into GFP(+)mice; the scaffold without cells was used as the control. Fluorescence imaging and histology revealed only allogeneic cells on the scaffold after 6 weeks and 12 weeks, and newly formed bone-like tissue from seeded cells was detected by 12 weeks. The presence of vessels was confirmed by CD31 immunohistochemical staining, which indicated the possibility of vessel formation from seeded MSCs.

However, there were four major drawbacks of their study. First, the use of Hoechst stain in fluorescence imaging to indicate seeded or host cells is not reasonable because the GFP harvest of cells may decay after transplantation for 6 weeks or 12 weeks; cells with GFP may

436 also stain with blue color, providing misleading results about the origin of cells. Second, the
437 surface view of fluorescence imaging cannot represent the actual cell interactions during bone
438 regeneration inside the 3-D scaffold. Third, the creation of only one defect in each mouse cannot
439 eliminate individual variations. Fourth, bone formation was supposed to be similar in both
440 experimental groups. The authors explained that GFP itself may be immunogenic in
441 immunocompetent mice; however, GFP was present in both groups.

442 To the best of the authors' knowledge, the present study is the first to compare the
443 distribution and proportion of seeded cells and host cells by tracking two fluorescent cells in the
444 same scaffold in a pig critical-sized calvarial defect model.

445 To eliminate individual variations in the animal study, we used a critical-sized calvarial
446 defect in pigs instead of rats due to the limited size of rats. As an animal model, we chose the
447 domestic pig because its bone regeneration rates correlate well with those found in humans (pigs
448 1.2 -1.5 mm per day, humans 1.0 - 1.5 mm per day) [34]. Numerous experiments have been
449 conducted to analyze bone formation with various scaffolds and factors in critical-sized calvarial
450 defect pigs [50-52] because of the uniform, flat and surgically feasible calvarial bone. In general,
451 a defect size with a diameter of at least 6mm is thought to be a reasonable critical-sized calvarial
452 defect, and we also used an empty group (group 1) as a control.

453 The CAG hybrid promoter-driven EGFP-MSCs derived from the transgenic pigs used in
454 this study have been proved to exhibit homogeneous surface epitopes and possess classic
455 trilineage differentiation potential into osteogenic, adipogenic, and chondrogenic lineages, with

456 robust EGFP expression maintained in all differentiated progeny. These cells have the major
457 advantage of greater sustained EGFP expression in stem cells and in all their differentiated
458 progeny [19] compared to GFP expression in transgenic pigs under the control of housekeeping
459 regulatory sequences [53,54].Increased expression of green fluorescence was observed from day
460 3 to day 28 after culture into scaffolds (Fig 4.and 6)

461 The transgenic Ds-Red pigs were produced by using pronuclear microinjection, and the
462 transgene comprised a CMV enhancer/chicken-beta actin promoter and DsRed monomeric
463 cDNA [33]. DsRed is a red fluorescent protein that was originally discovered in corals of the
464 class Anthozoa. DsRed is expressed ubiquitously, with red fluorescence detected in the brain,
465 eye, tongue, heart, lung, liver, pancreas, spleen, stomach, small intestine, large intestine, kidney,
466 testis, and muscle, as confirmed by histology and western blot analyses. Red fluorescence
467 tracking was previously applied in transplantation of neurons from Ds-Red transgenic pigs into a
468 Parkinson's disease rat model [55]. In this *in vivo* experiment, precise evaluation and analysis
469 could be achieved due to the abundant expression of the two fluorescent proteins in all
470 differentiated progeny.

471 The hemostatic gelatin sponge, Spongostan™, is prepared from purified type A pork
472 skin, and its biosafety in clinical applications, especially to control bleeding during surgery, has
473 long been proved [56, 57]. *In vivo* studies have shown good biocompatibility of Spongostan™
474 without any immune response during bone formation [36]. The main reasons that we chose this
475 scaffold are its biocompatibility and biodegradation with MSCs and absence of autofluorescence

476 [36].

477 Our *in vivo* fluorescence analysis (Fig 9 and 10) showed that the green fluorescence in
478 the scaffold loaded with seeded cells in groups 4 and 5 was significantly higher than that in the
479 other groups from week 1 to week 4, which means that the seeded cells did play an important
480 role in the osteogenic differentiation process. EGFP-pMSCs were highest in group 5 in the 4th
481 week, which means that the higher load of seeded cells was sustained until the 4th week. DsRed
482 expression (Fig10) was highest in Group 4 in the 1st week, indicating that recruitment [58, 59] of
483 host cells was facilitated in the lower density-seeded scaffold than the empty scaffold or higher
484 density-seeded scaffold. DsRed expression decreased from the 1st week to 4th week in group 4
485 but increased in group 5, which means that more EGFP-pMSCs can recruit more host cells in the
486 following period and that enough available space and higher cell loading benefit tissue
487 regeneration. The higher expression of EGFP and DsRed fluorescence in groups 4 and 5 were
488 compatible with the histological results, which indicated more obvious deposition of osteoids in
489 groups 4 and 5 in week 4. The immunohistochemical results for CD68 in week 4 also showed
490 obvious osteogenesis in groups 4 and 5.

491 Our *in vivo* results demonstrated that the seeded MSCs promoted host cell migration,
492 which contributed to the higher number of host cells in the transplanted scaffolds. In addition,
493 according to the histological staining, we found that the percentage of osteoid formation in the
494 scaffolds transplanted with seeded MSCs was significantly higher than that in the control group,
495 which means that not only the transplanted seeded cells but also the recruited host cells

contributed to the entire process.

In summary, we found that more seeded cells recruit more host cells and that both cell types participate in osteogenesis. Recruitment of host cells was facilitated in the lower density-seeded scaffold than the empty scaffold or higher density-seeded scaffold in the first week but sustained recruitment of host cells was achieved in higher density-seeded scaffold and result in more obvious deposition of osteoids. Scaffolds without seeded cells may therefore not be effective in bone transplantation based on this *in vivo* study.

Acknowledgments

This work was supported by the Chang Gung Memorial Hospital (grant No. CMRPG3G2061 ; CMRPG3G0572). We would like to thank the Microscope Core Laboratory at the Center for Advanced Molecular Imaging and Translation and the Laboratory Animal Center of Linko Chang Gung Memorial Hospital.

References

1. Bhumiratana S, Vunjak-Novakovic G. Concise review: personalized human bone grafts for reconstructing head and face. Stem Cells Transl Med. 2012;1: 64-69.

2. Bauer TW, Muschler GF. Bone graft materials. An overview of the basic science. Clin Orthop Relat Res. 2000;371: 10-27.

3. Kuznetsova D, Timashev P, Bagratashvili VN, Zagaynova EV. Scaffold- and cell system-based bone grafts in tissue engineering (review). Sovrem Tehnologii Med. 2014;6: 201-211.

4. Chan BP, Leong KW. Scaffolding in tissue engineering: general approaches and tissue-specific considerations. Eur Spine J. 2008;17: 467-479.

5. Ryu SI, Lim JT, Kim S-M, Paterno J, Kim DH. Comparison of the biomechanical stability of dense cancellous allograft with tricortical iliac autograft and fibular allograft for cervical interbody fusion. Eur Spine J. 2006;15: 1339-1345.

6. Godzik J, Ravindra VM, Ray WZ, Schmidt MH, Bisson EF, Dailey AT. Comparison of structural allograft and traditional autograft technique in occipitocervical fusion: radiological and clinical outcomes from a single institution. J Neurosurg Spine. 2015;23: 144-152.

7. Knapp DR, Jones ET, Blanco JS, Flynn JC, Price CT. Allograft bone in spinal fusion for adolescent idiopathic scoliosis. J Spinal Disord Tech. 2005;18: S73-S76.

8. Jones KC, Andrish J, Kuivila T, Gurd A. Radiographic outcomes using freeze-dried

cancellous allograft bone for posterior spinal fusion in pediatric idiopathic scoliosis. J Pediatr Orthop. 2002;22: 285-289.

9. Cabraja M, Kroppenstedt S. Bone grafting and substitutes in spine surgery. J Neurosurg Sci. 2012;56: 87-95.

10. Rihn JA, Kirkpatrick K, Albert TJ. Graft options in posterolateral and posterior interbody lumbar fusion. Spine. 2010;35: 1629-1639.

11. Andersen T, Christensen FB, Niedermann B, Helmig P, Hoy K, Hansen ES, et al. Impact of instrumentation in lumbar spinal fusion in elderly patients: 71 patients followed for 2-7 years. Acta Orthop. 2009;80: 445-450.

12. Ploumis A, Albert TJ, Brown Z, Mehbod AA, Transfeldt EE. Healos graft carrier with bone marrow aspirate instead of allograft as adjunct to local autograft for posterolateral fusion in degenerative lumbar scoliosis: a minimum 2-year follow-up study. J Neurosurg Spine. 2010;13: 211-215.

13. Arnold PM, Robbins S, Paullus W, Faust S, Holt R, McGuire R. Clinical outcomes of lumbar degenerative disc disease treated with posterior lumbar interbody fusion allograft spacer: a prospective, multicenter trial with 2-year follow-up. Am J Orthop (Belle Mead NJ). 2009;38: E115-E122.

14. Slosar PJ, Josey R, Reynolds J. Accelerating lumbar fusions by combining rhBMP-2 with allograft bone: a prospective analysis of interbody fusion rates and clinical outcomes. Spine J. 2007;7: 301-307.

15. Faundez AA, Schwender JD, Safriel Y, Gilbert TJ, Mehbod AA, Denis F, et al. Clinical and radiological outcome of anterior-posterior fusion versus transforaminal lumbar interbody fusion for symptomatic disc degeneration: a retrospective comparative study of 133 patients. Eur Spine J. 2009;18: 203-211.

16. Buser Z, Brodke DS, Youssef JA, Rometsch E, Park JB, Yoon ST, et al. Allograft versus demineralized bone matrix in instrumented and noninstrumented lumbar fusion: a systematic review. Global Spine J. 2018;8: 396-412.

17. Ohyama M, Okano H. Promise of human induced pluripotent stem cells in skin regeneration and investigation. J Invest Dermatol. 2014;134: 605-609.

18. Michel J, Penna M, Kochen J, Cheung H. Recent advances in hydroxyapatite scaffolds containing mesenchymal stem cells. Stem Cells Int. 2015;2015: 1-13.

19. Hsiao FS, Lian WS, Lin SP, Lin CJ, Lin YS, Cheng EC, et al. Toward an ideal animal model to trace donor cell fates after stem cell therapy: production of stably labeled multipotent mesenchymal stem cells from bone marrow of transgenic pigs harboring enhanced green fluorescence protein gene. J Anim Sci. 2011;89: 3460-3472.

20. Arpornmaeklong P, Brown SE, Wang Z, Krebsbach PH. Phenotypic characterization, osteoblastic differentiation, and bone regeneration capacity of human embryonic stem cell-derived mesenchymal stem cells. Stem Cells Dev. 2009;18: 955-968.

21. Lee JY, Choo JE, Choi YS, Shim IK, Lee SJ, Seol YJ, et al. Effect of immobilized cell-binding peptides on chitosan membranes for osteoblastic differentiation of mesenchymal

stem cells. Biotechnol Appl Biochem. 2009;52: 69-77.

22. Amini AR, Laurencin CT, Nukavarapu SP. Bone tissue engineering: recent advances and challenges. Crit Rev Biomed Eng. 2012;40: 363-408.

23. Mauney JR, Volloch V, Kaplan DL. Role of adult mesenchymal stem cells in bone tissue engineering applications: current status and future prospects. Tissue Eng. 2005;11: 787-802.

24. Tasso R, Ulivi V, Reverberi D, lo Sicco C, Descalzi F, Cancedda R. *In vivo* implanted bone marrow-derived mesenchymal stem cells trigger a cascade of cellular events leading to the formation of an ectopic bone regenerative niche. Stem Cells Dev. 2013;22: 3178-3191.

25. Gamblin AL, Brennan MA, Renaud A, Yagita H, Lezot F, Heymann D, et al. Bone tissue formation with human mesenchymal stem cells and biphasic calcium phosphate ceramics: the local implication of osteoclasts and macrophages. Biomaterials. 2014;35: 9660-9667.

26. Kulkarni M, Greiser U, O'Brien T, Pandit A. Liposomal gene delivery mediated by tissue-engineered scaffolds. Trends Biotechnol. 2010;28: 28-36.

27. Lei Y, Segura T. DNA delivery from matrix metalloproteinase degradable poly(ethylene glycol) hydrogels to mouse cloned mesenchymal stem cells. Biomaterials. 2009;30: 254-265.

28. Sun XD, Jeng L, Bolliet C, Olsen BR, Spector M. Non-viral endostatin plasmid transfection of mesenchymal stem cells via collagen scaffolds. Biomaterials. 2009;30:

1222-1231.

29. Mulder G, Tallis AJ, Marshall VT, Mozingo D, Phillips L, Pierce GF, et al. Treatment of nonhealing diabetic foot ulcers with a platelet-derived growth factor gene-activated matrix (GAM501): results of a phase 1/2 trial. Wound Repair Regen. 2009;17: 772-779.

30. Sapet C, Formosa C, Sicard F, Bertosio E, Zelphati O, Laurent N. 3D-fection: cell transfection within 3D scaffolds and hydrogels. Ther Deliv. 2013;4: 673-685.

31. Villa MM, Wang L, Rowe DW, Wei M. Effects of cell-attachment and extracellular matrix on bone formation *in vivo* in collagen-hydroxyapatite scaffolds. PLoS One. 2014;9: e109568.

32. Jensen J, Tvedesoe C, Rolfing JH, Foldager CB, Lysdahl H, Kraft DC, et al. Dental pulp-derived stromal cells exhibit a higher osteogenic potency than bone marrow-derived stromal cells *in vitro* and in a porcine critical-size bone defect model. SICOT J. 2016;2: 16.

33. Chou C-J, Peng S-Y, Wu M-H, Yang C-C, Lin Y-S, Cheng WT-K, et al. Generation and characterization of a transgenic pig carrying a DsRed-monomer reporter gene. PLoS One. 2014;9: e106864.

34. Schlegel KA, Lang FJ, Donath K, Kulow JT, Wiltfang J. The monocortical critical size bone defect as an alternative experimental model in testing bone substitute materials. Oral Surg Oral Med Oral Pathol Oral Radiol Endod. 2006;102: 7-13.

35. Wehrhan F, Amann K, Molenberg A, Lutz R, Neukam FW, Schlegel KA. PEG matrix

enables cell-mediated local BMP-2 gene delivery and increased bone formation in a porcine critical size defect model of craniofacial bone regeneration. Clin Oral Implants Res. 2012;23: 805-813.

36. Kuo Z-K, Lai P-L, Toh EK-W, Weng C-H, Tseng H-W, Chang P-Z, et al. Osteogenic differentiation of preosteoblasts on a hemostatic gelatin sponge. Sci Rep. 2016;6: 32884.

37. Hsieh M-K, Wu C-J, Chen C-C, Tsai T-T, Niu C-C, Wu S-C, et al. BMP-2 gene transfection of bone marrow stromal cells to induce osteoblastic differentiation in a rat calvarial defect model. Mater Sci Eng C. 2018;91: 806-816.

38. Mangano C, de Rosa A, Desiderio V, d'Aquino R, Piattelli A, de Francesco F, et al. The osteoblastic differentiation of dental pulp stem cells and bone formation on different titanium surface textures. Biomaterials. 2010;31: 3543-3551.

39. Ito K, Yamada Y, Nakamura S, Ueda M. Osteogenic potential of effective bone engineering using dental pulp stem cells, bone marrow stem cells, and periosteal cells for osseointegration of dental implants. Int J Oral Maxillofac Implants. 2011;26: 947-954.

40. Qin Y, Guan J, Zhang C. Mesenchymal stem cells: mechanisms and role in bone regeneration. Postgrad Med J. 2014;90: 643-647.

41. Patel D, Shah J, Srivastava A. Therapeutic potential of mesenchymal stem cells in regenerative medicine. Stem Cells Int 2013;49: 21-28.

42. Koob S, Torio-Padron N, Stark GB, Hannig C, Stankovic Z, Finkenzeller G. Bone formation and neovascularization mediated by mesenchymal stem cells and endothelial

cells in critical-sized calvarial defects. Tissue Eng Part A. 2011;17: 311-321.

43. Nassif L, Sabban M. Mesenchymal stem cells in combination with scaffolds for bone tissue engineering. Materials (Basel). 2011;4: 1793-1804.

44. Kwon DY, Kwon JS, Park SH, Park JH, Jang SH, Yin XY, et al. A computer-designed scaffold for bone regeneration within cranial defect using human dental pulp stem cells. Sci Rep. 2015;5: 12721.

45. Kargozar S, Mozafari M, Hashemian SJ, Milan P, Hamzehlou S, Soleimani M, et al. Osteogenic potential of stem cells-seeded bioactive nanocomposite scaffolds: a comparative study between human mesenchymal stem cells derived from bone, umbilical cord Wharton's jelly, and adipose tissue. J Biomed Mater Res B Appl Biomater. 2018;106: 61-72.

46. Raftery RM, Mencia-Castano I, Sperger S, Chen G, Cavanagh B, Feichtinger GA, et al. Delivery of the improved BMP-2-Advanced plasmid DNA within a gene-activated scaffold accelerates mesenchymal stem cell osteogenesis and critical size defect repair. J Control Release. 2018;283: 20-31.

47. Guo J, Wu G. The signaling and functions of heterodimeric bone morphogenetic proteins. Cytokine Growth Factor Rev. 2012;23: 61-67.

48. Annamalai RT, Turner PA, Carson WF, Levi B, Kunkel S, Stegemann JP. Harnessing macrophage-mediated degradation of gelatin microspheres for spatiotemporal control of BMP2 release. Biomaterials. 2018;161: 216-227.

650 49. Kuznetsova D, Prodanets N, Rodimova S, Antonov E, Meleshina A, Timashev P, et al.
651 Study of the involvement of allogeneic MSCs in bone formation using the model of
652 transgenic mice. Cell Adh Migr. 2016;11: 233-244.
653 50. Park J, Lutz R, Felszeghy E, Wiltfang J, Nkenke E, Neukam FW, et al. The effect on
654 bone regeneration of a liposomal vector to deliver BMP-2 gene to bone grafts in peri-
655 implant bone defects. Biomaterials. 2007;28: 2772-2782.
656 51. Stockmann P, Park J, von Wilmowsky C, Nkenke E, Felszeghy E, Dehner JF, et al.
657 Guided bone regeneration in pig calvarial bone defects using autologous mesenchymal
658 stem/progenitor cells - a comparison of different tissue sources. J Craniomaxillofac Surg.
659 2012;40: 310-320.
660 52. Bornstein MM, Heynen G, Bosshardt DD, Buser D. Effect of two bioabsorbable barrier
661 membranes on bone regeneration of standardized defects in calvarial bone: a comparative
662 histomorphometric study in pigs. J Periodontol. 2009;80: 1289-1299.
663 53. Nowak-Imialek M, Kues WA, Petersen B, Lucas-Hahn A, Herrmann D, Haridoss S, et al.
664 Oct4-enhanced green fluorescent protein transgenic pigs: a new large animal model for
665 reprogramming studies. Stem Cells Dev. 2011;20: 1563-1575.
666 54. Yong HY, Hao Y, Lai L, Li R, Murphy CN, Rieke A, et al. Production of a transgenic
667 piglet by a sperm injection technique in which no chemical or physical treatments were
668 used for oocytes or sperm. Mol Reprod Dev. 2006;73: 595-599.
669 55. Chiu CH, Li IH, Weng SJ, Huang YS, Wu SC, Chou TK, et al. PET imaging of serotonin

transporters with 4-[(18)F]-ADAM in a parkinsonian rat model with porcine neural xenografts. Cell Transplant. 2016;25: 301-311.

56. Seo JP, Tsuzuki N, Haneda S, Yamada K, Furuoka H, Tabata Y, et al. Osteoinductivity of gelatin/beta-tricalcium phosphate sponges loaded with different concentrations of mesenchymal stem cells and bone morphogenetic protein-2 in an equine bone defect model. Vet Res Commun. 2014;38: 73-80.

57. Amjadian S, Seyedjafari E, Zeynali B, Shabani I. The synergistic effect of nano-hydroxyapatite and dexamethasone in the fibrous delivery system of gelatin and poly(l-lactide) on the osteogenesis of mesenchymal stem cells. Int J Pharm. 2016;507: 1-11.

58. Lin W, Xu L, Zwingenberger S, Gibon E, Goodman SB, Li G. Mesenchymal stem cells homing to improve bone healing. J Orthop Translat. 2017;9: 19-27.

59. Xu L, Huang S, Hou Y, Liu Y, Ni M, Meng F, et al. Sox11-modified mesenchymal stem cells (MSCs) accelerate bone fracture healing: sox11 regulates differentiation and migration of MSCs. FASEB J. 2015;29: 1143-1152.

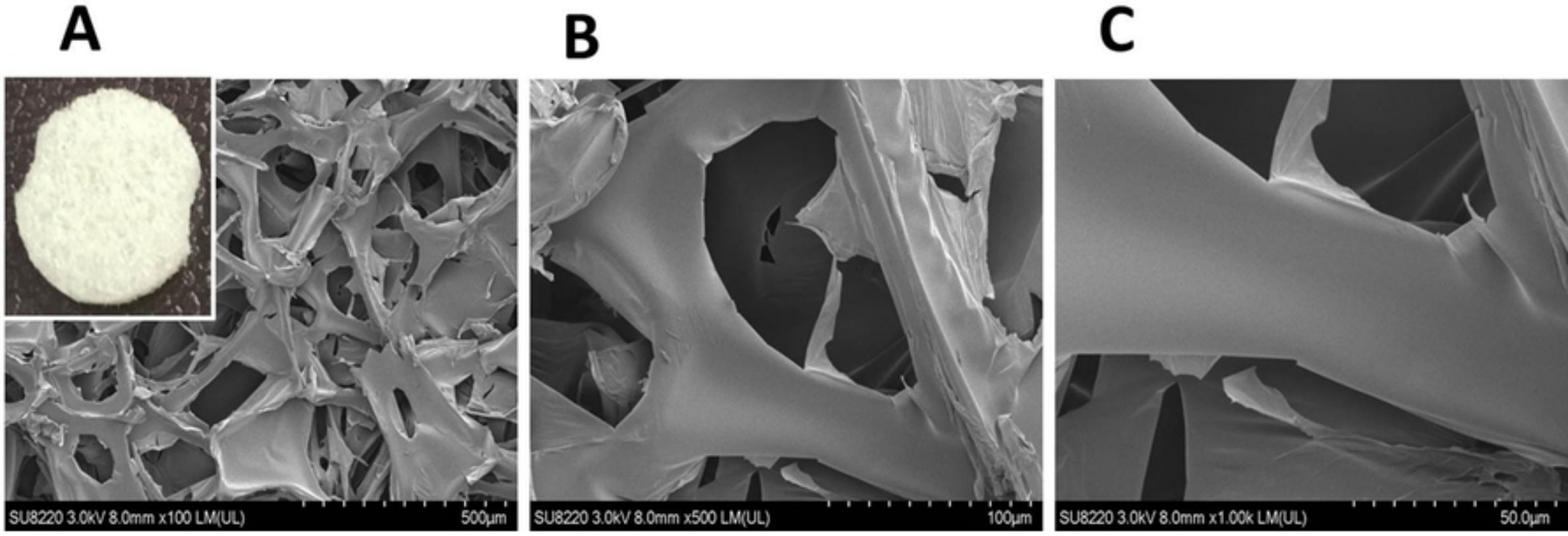
A
B
C
SU8220 3.0kV 8.0mm x100 LM(UL)
500µm
SU8220 3.0kV 8.0mm x500 LM(UL)
100µm
SU8220 3.0kV 8.0mm x1.00k LM(UL)
50.0µm

Figure1

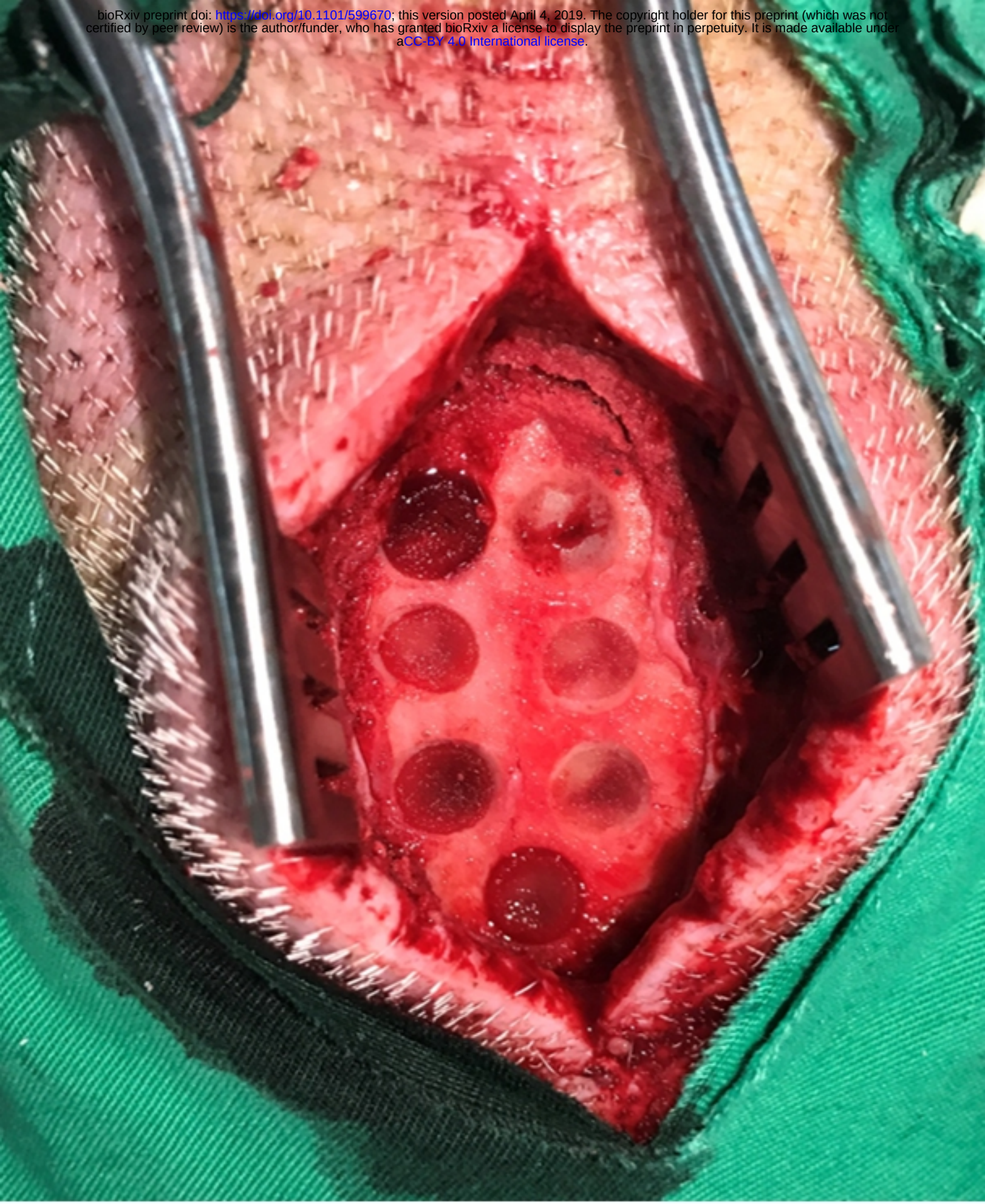

Figure2

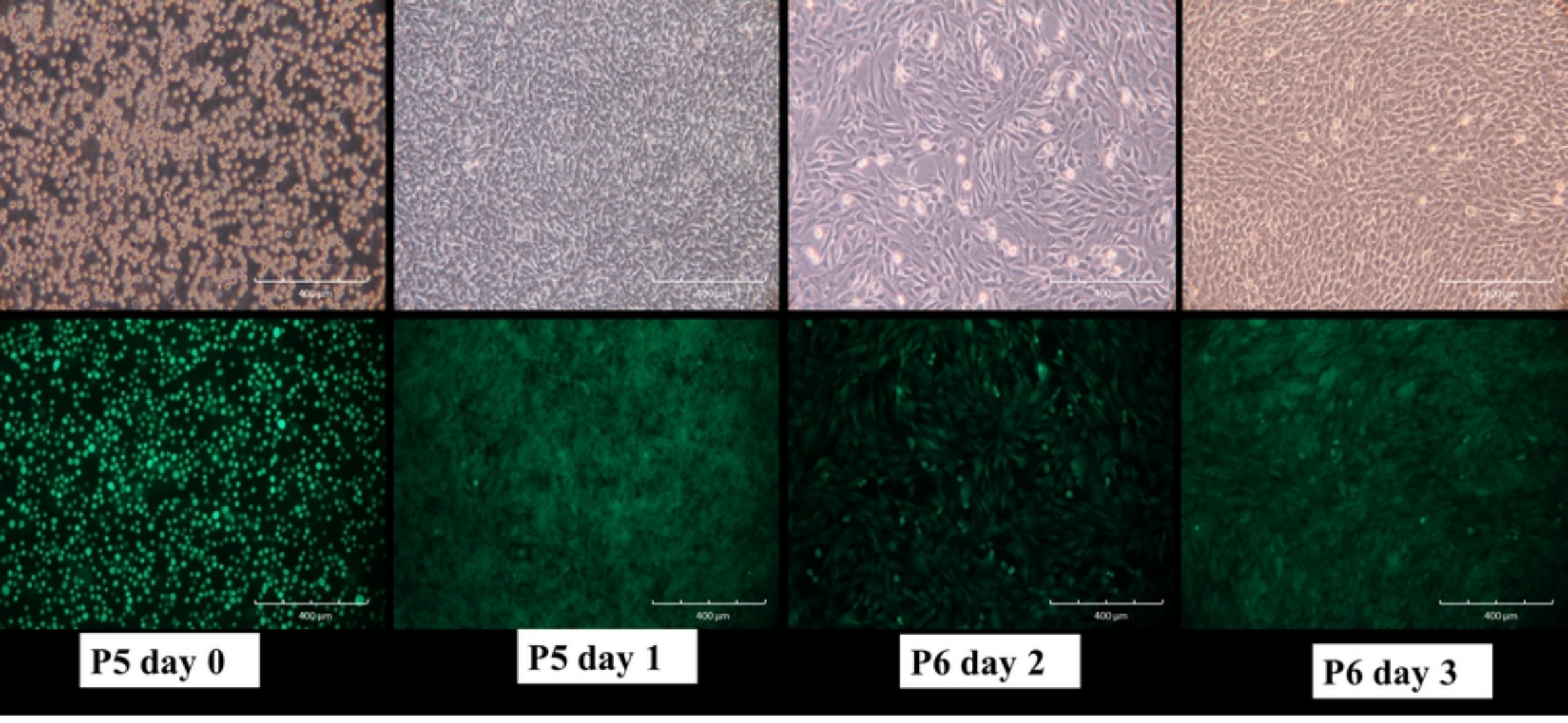

Figure3

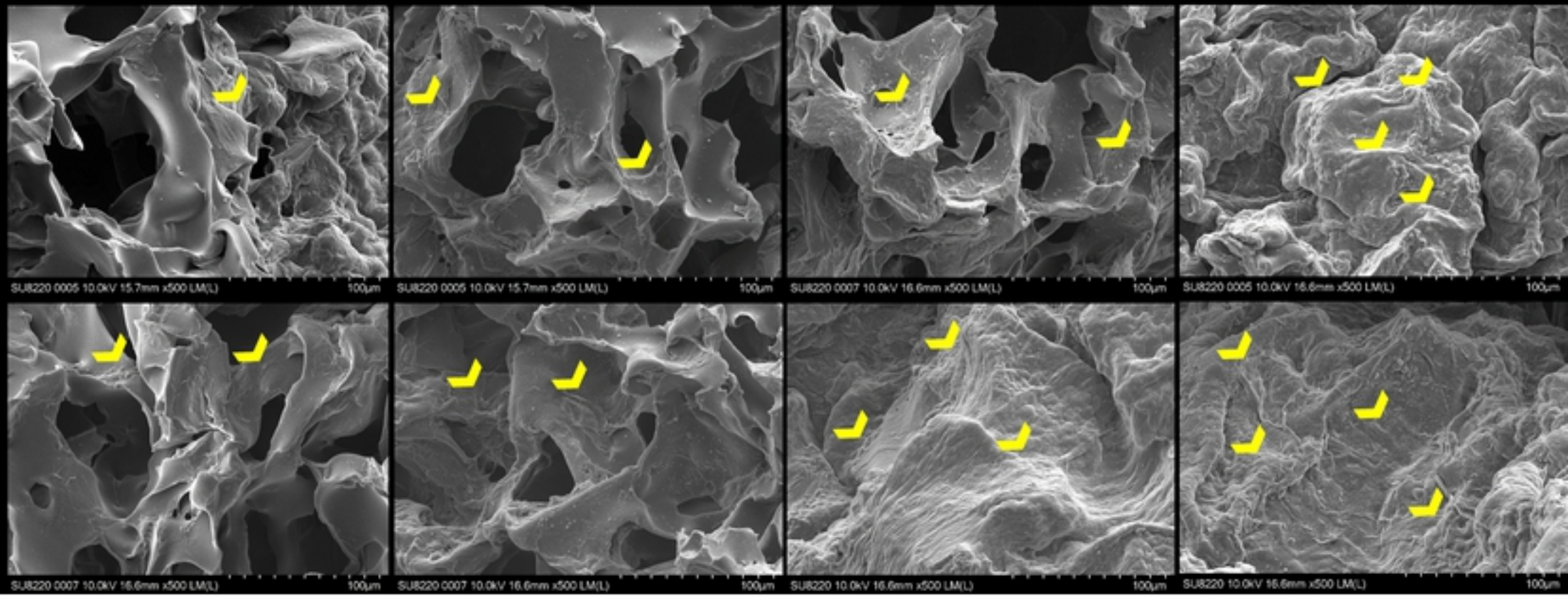
SU8220 0005 10.0kV 15.7mm x500 LM(L) 100μm
SU8220 0005 10.0kV 15.7mm x500 LM(L) 100μm
SU8220 0007 10.0kV 16.6mm x500 LM(L) 100μm
SU8220 0005 10.0kV 16.6mm x500 LM(L) 100μm
SU8220 0007 10.0kV 16.6mm x500 LM(L) 100μm
SU8220 0007 10.0kV 16.6mm x500 LM(L) 100μm
SU8220 10.0kV 16.6mm x500 LM(L) 100μm
SU8220 10.0kV 16.6mm x500 LM(L) 100μm

Figure5

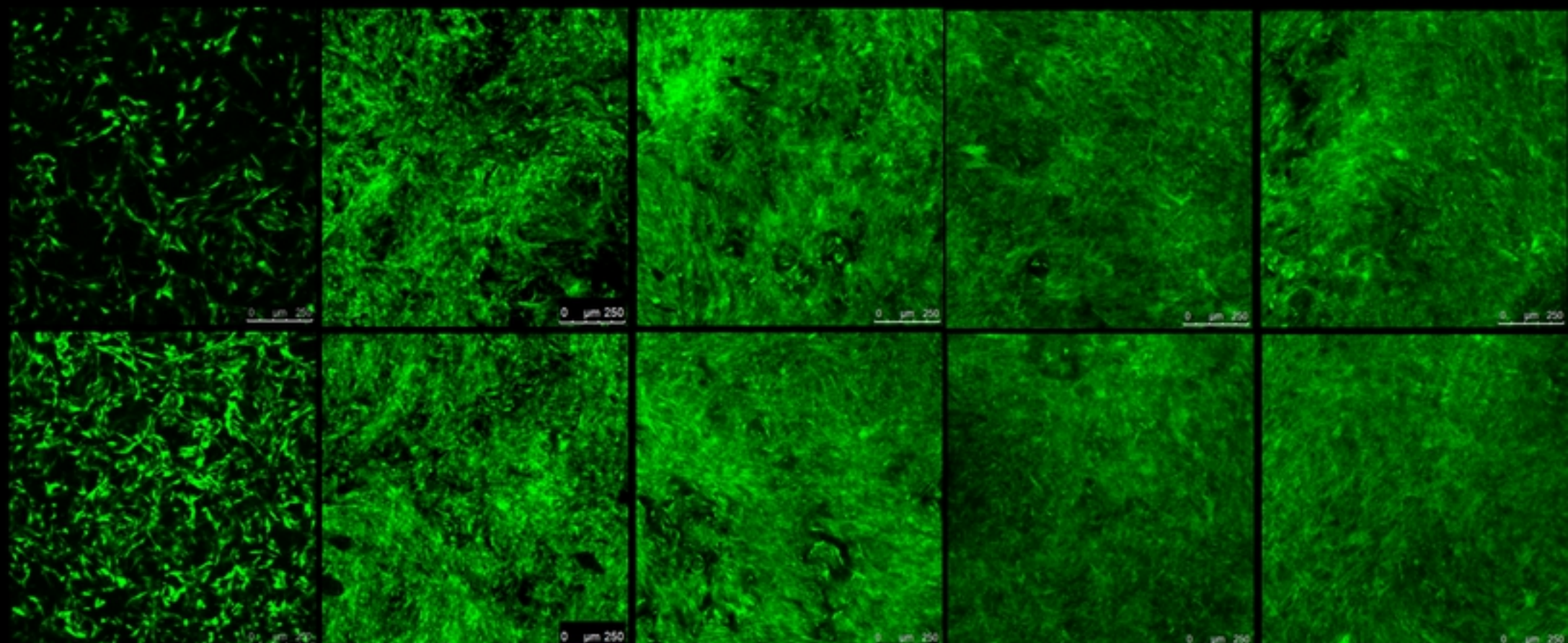

Figure6A

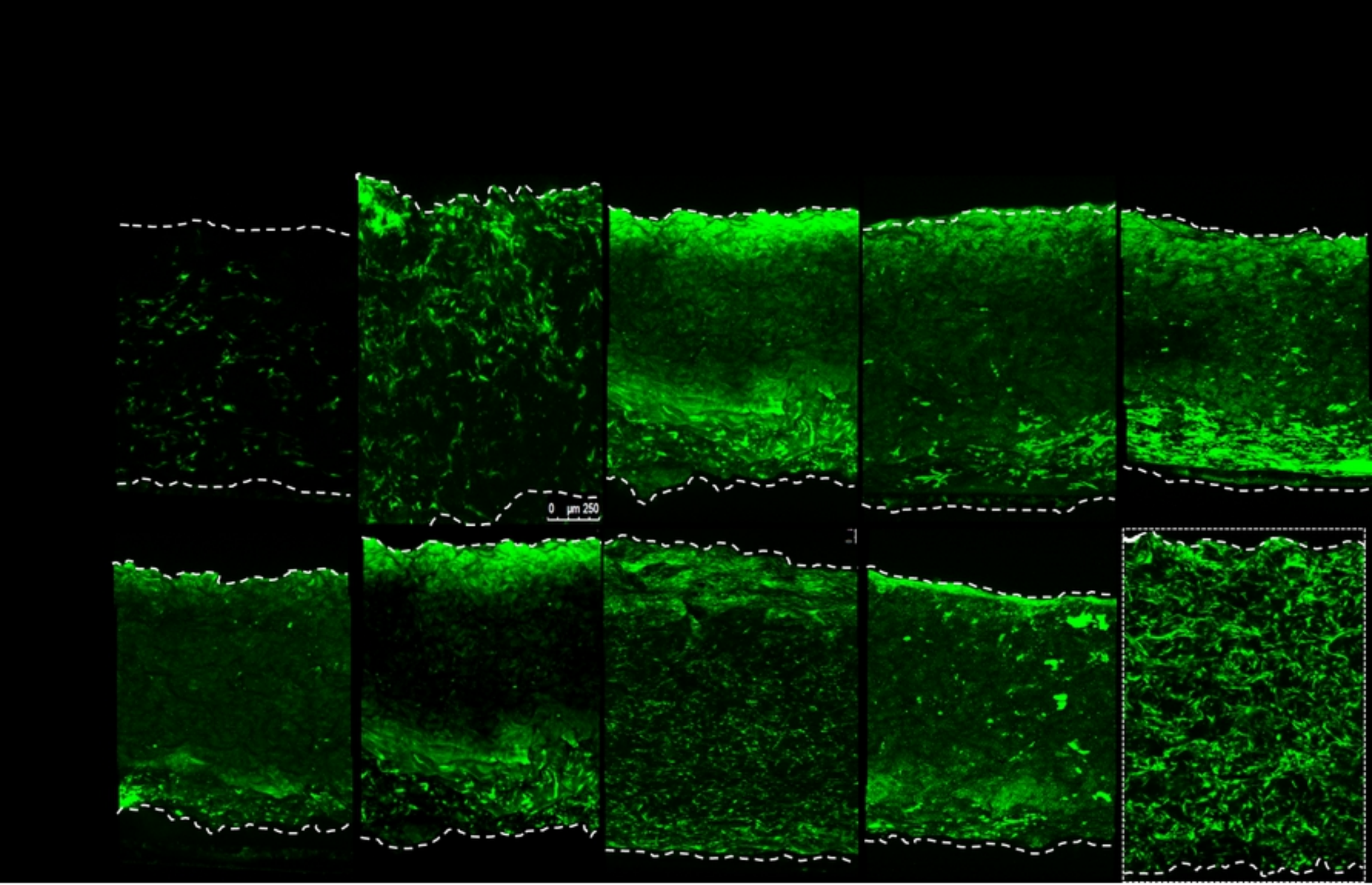

Figure6B

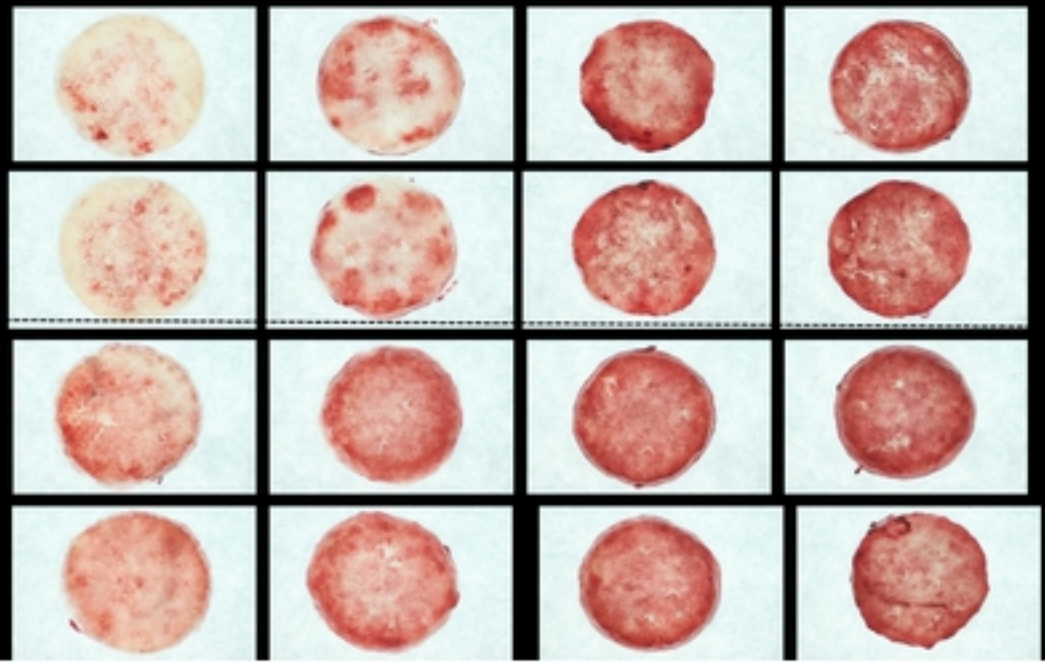

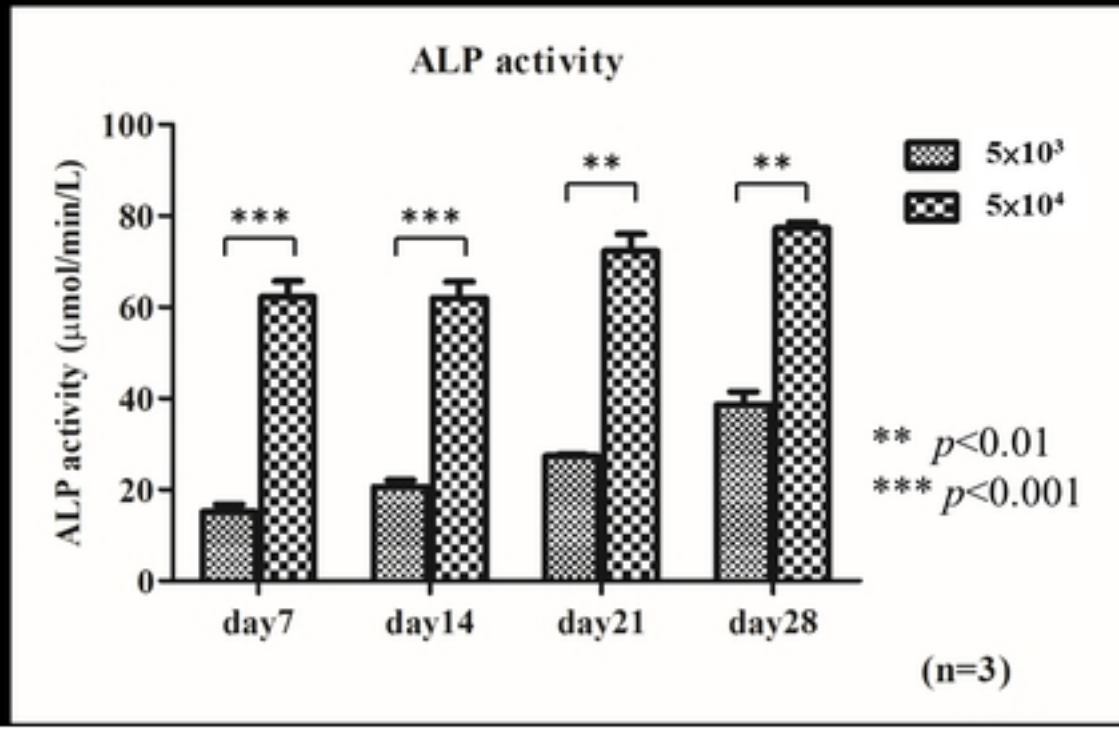
ALP activity
ALP activity (μmol/min/L)
100
80
60
40
20
0
***
***
**
**
day7
day14
day21
day28
5x10³
5x10⁴
** p<0.01
*** p<0.001
(n=3)

Figure7

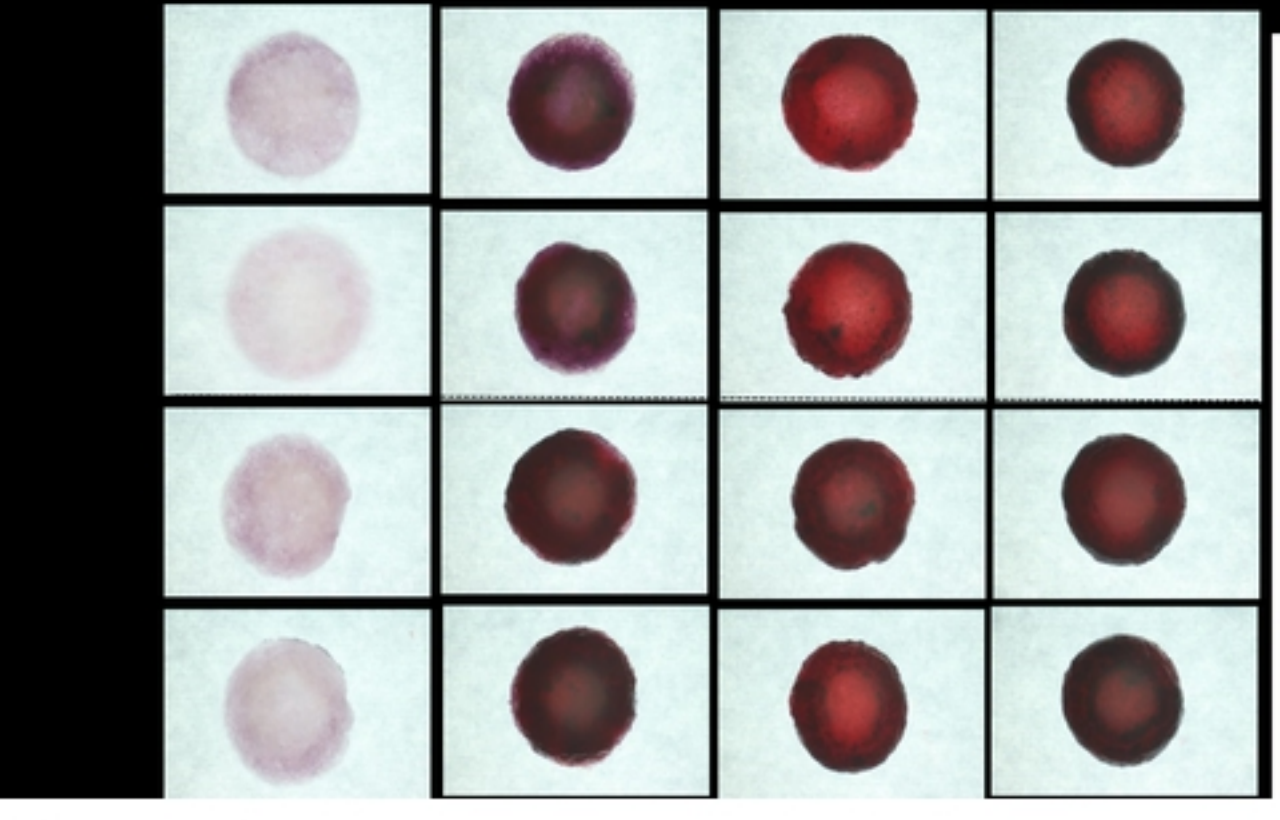

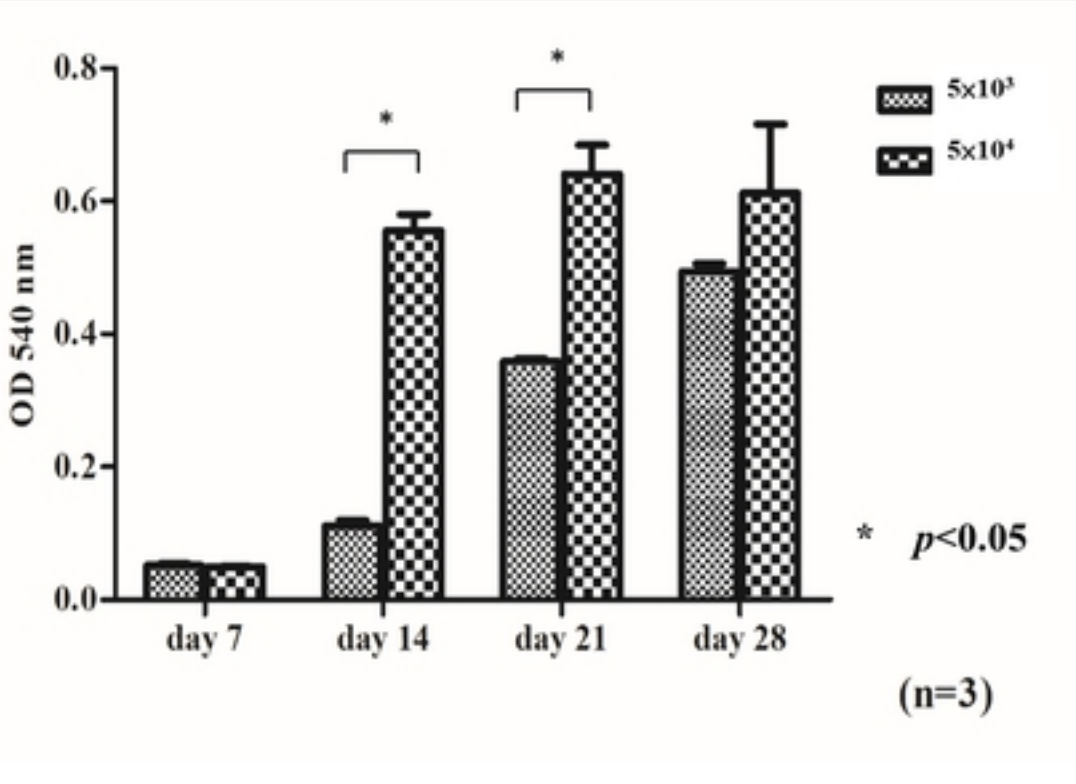
0.8
0.6
0.4
0.2
0.0
OD 540 nm
*
*
day 7
day 14
day 21
day 28
5x10³
5x10⁴
* p<0.05
(n=3)

Figure8

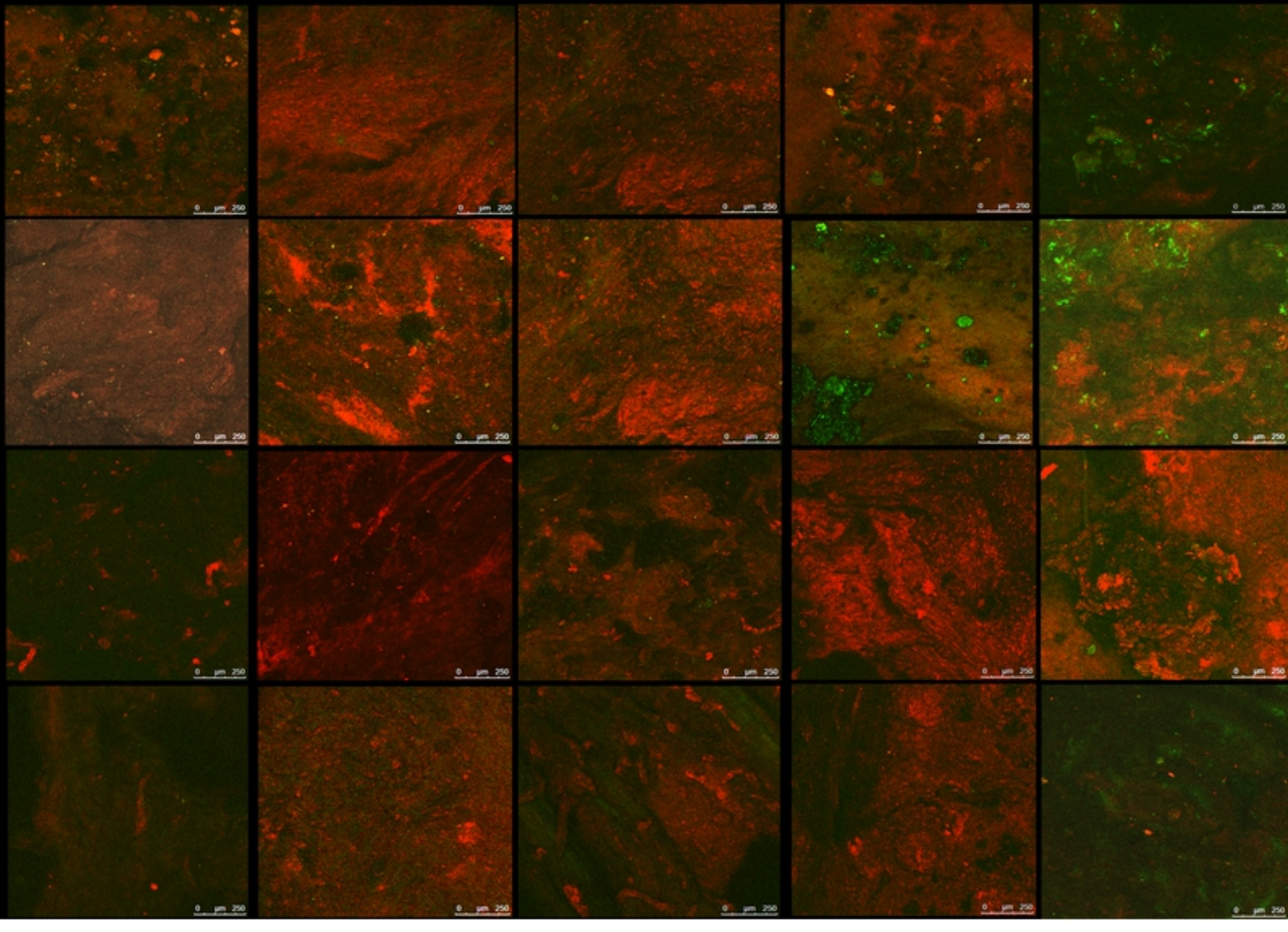

Figure9

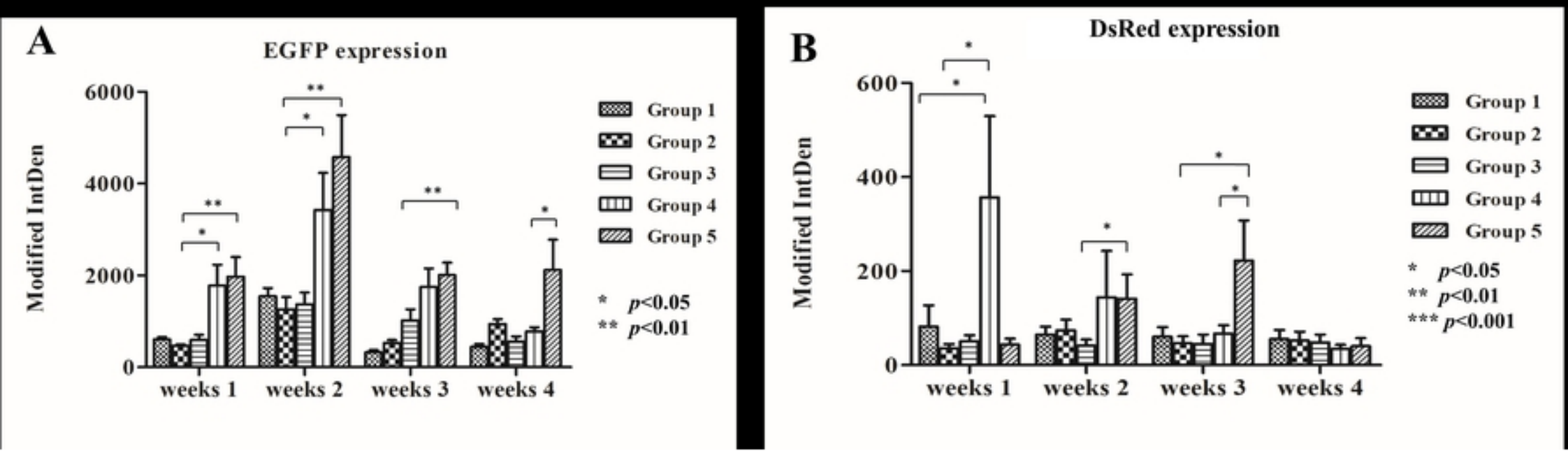
A
EGFP expression
Modified IntDen
6000
4000
2000
0
weeks 1
weeks 2
weeks 3
weeks 4
Group 1
Group 2
Group 3
Group 4
Group 5
* p<0.05
** p<0.01
B
DsRed expression
Modified IntDen
600
400
200
0
weeks 1
weeks 2
weeks 3
weeks 4
Group 1
Group 2
Group 3
Group 4
Group 5
* p<0.05
** p<0.01
*** p<0.001

Figure10

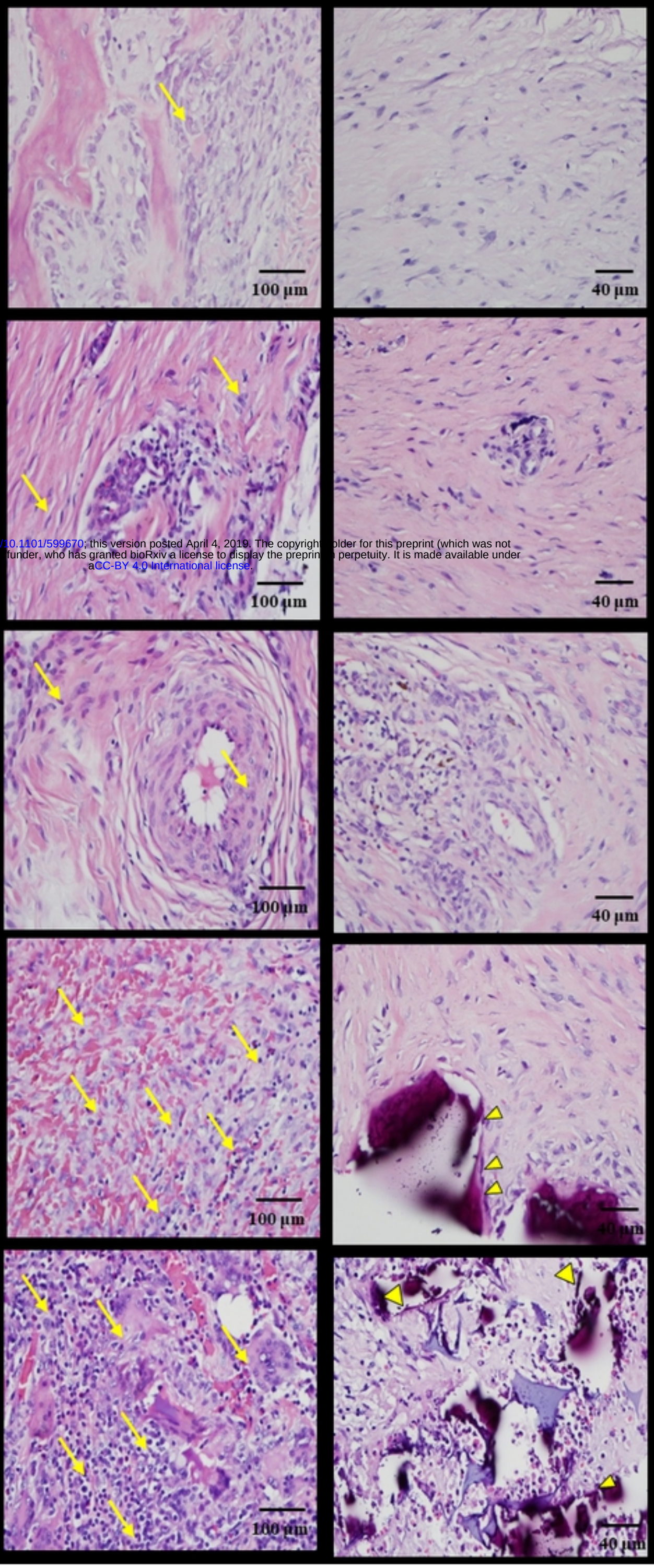

Figure11

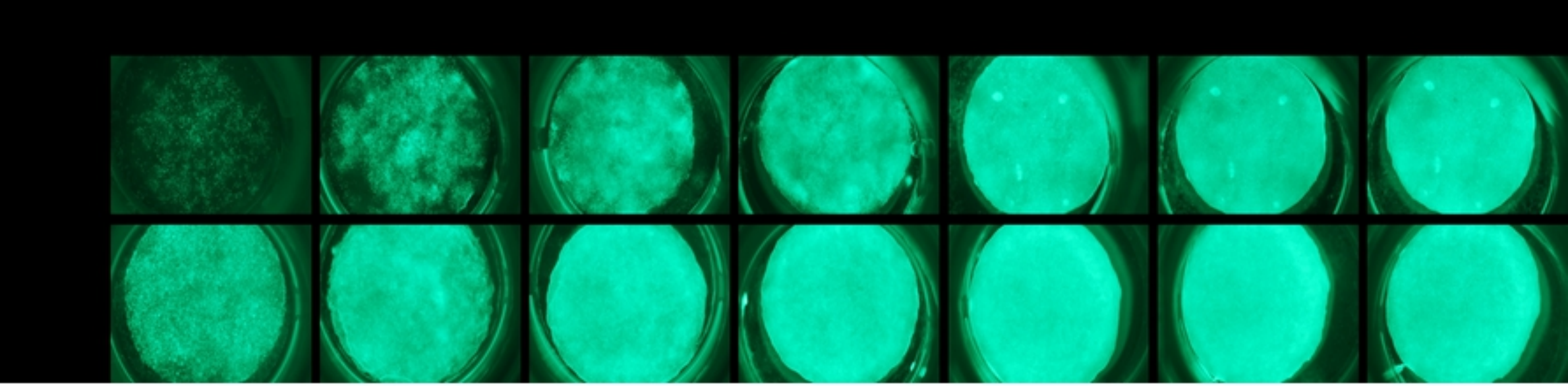

Figure4

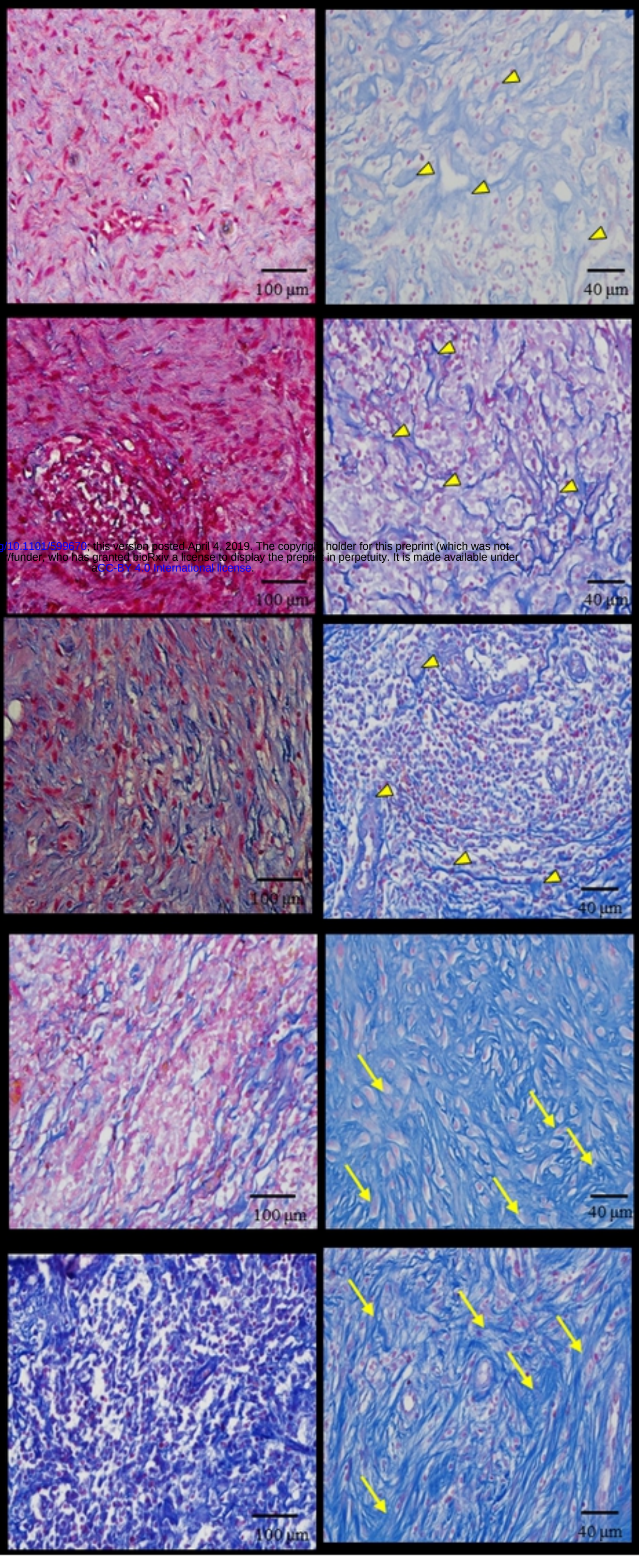

Figure12

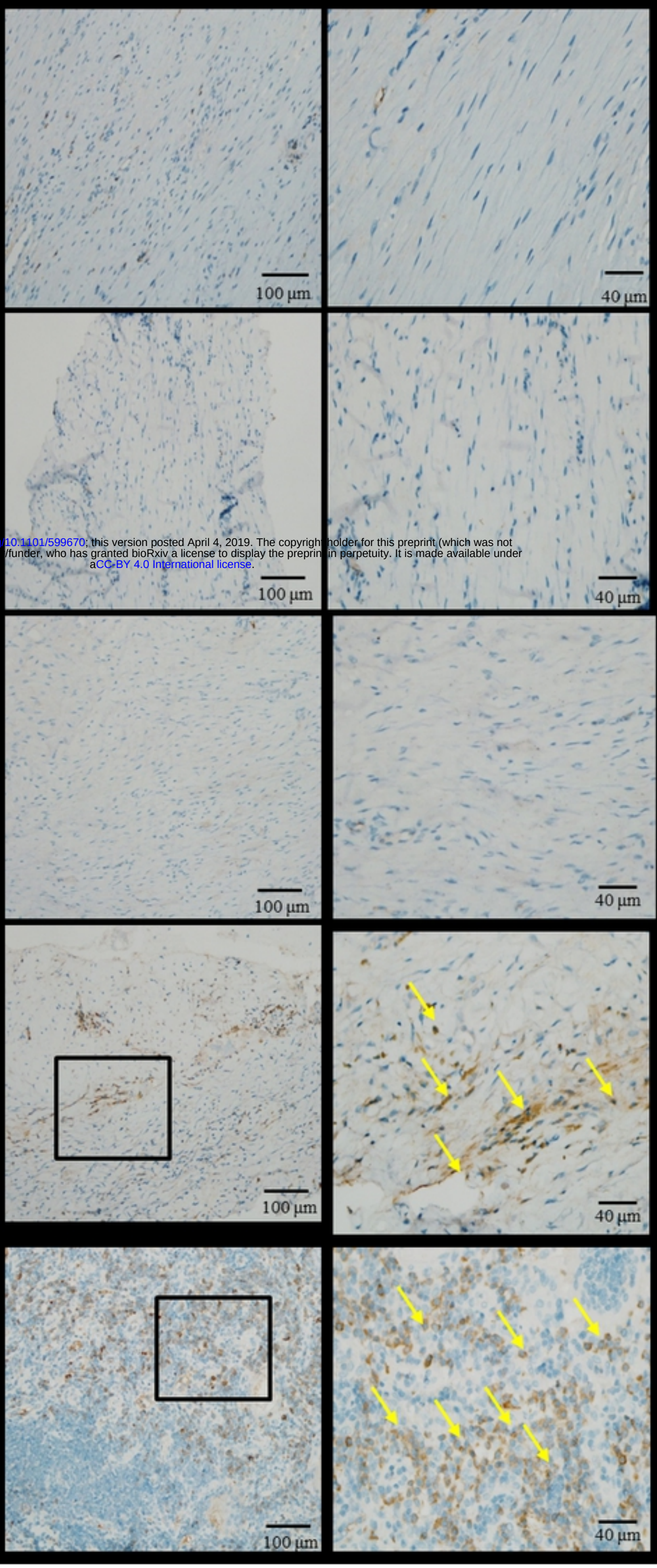

Figure13